

pubs.acs.org/crystal Article

Crystallite Tuning of Magnetic Properties in S = 1/2 Ni(III) Cyclam (Bi)sulfate Complex Salts

Published as part of a Crystal Growth and Design virtual special issue on Molecular Magnets and Switchable Magnetic Materials

Thomas L. Morrison, Indrani Bhowmick, and Matthew P. Shores*



Cite This: Cryst. Growth Des. 2023, 23, 3186-3194



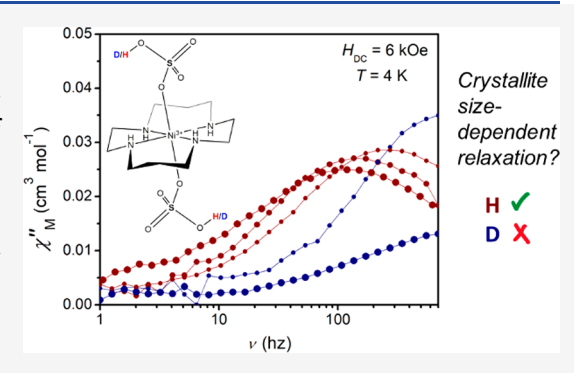
ACCESS

III Metrics & More

Article Recommendations

Supporting Information

ABSTRACT: Molecular-level crystallographic tuning of a coordination complex structure can enable manipulation of the small energies that govern intra- and intermolecular responses toward molecular actuators. Chemically tuning of the magnetic response of S=1/2 coordination complexes is of particular interest in recent years because these species represent the simplest electron-based quantum bits (qubits) for developing molecular quantum computers. In this report, we discuss the crystallographic tuning tools and corresponding magnetic properties of novel S=1/2 Ni(III) cyclam complex salts: strong antiferromagnetic coupling in sulfate-bridged chain $\{[Ni-(cyclam)(\mu^2-SO_4)]ClO_4\cdot H_2O\}_n$ (1) and field-, temperature-, and size-dependent slow magnetic relaxation in molecular $[Ni(cyclam)(HSO_4)_2]$ -HSO₄ (2). We have reported two methods of manipulating the dynamic



magnetic response of these coordination molecules: particle size selection and deuteration. We find that particle size dependency, which we attribute to the phonon bottleneck effect, for the magnetic dynamics in the parent compound 2, is removed in deuterated $2-\mathbf{d}_7$, revealing only the faster molecular relaxation mode(s).

■ INTRODUCTION

Mononuclear single-molecule magnets (SMMs) are promising for exploitation in emerging information science technologies as potential quantum bits (qubits), high density data storage, and gates for spin-polarized currents. While lanthanide SMMs currently feature higher operating temperatures, SMMs sourced from first-row transition metal ions are interesting due to their potential cost efficiency and increased sensitivity to local environments. Thus far, a handful of 3d coordination complexes, featuring V(IV), $^{9-11}$ Mn(IV), low spin Co(II), $^{13-15}$ Ni(I, III), 7,16 and Cu(II) ions, have been shown to possess slow magnetic relaxation in the S=1/2 state, providing an opportunity to design the smallest unit of molecular magnetic materials.

For SMMs with S > 1/2, there is an intrinsic (to the complex) barrier to transitions between microstates in the ground term; pathways for spin reorientation are governed by quantum tunneling through the barrier and/or energy absorption from various vibrations to go over the barrier. In contrast, for SMMs with S = 1/2 ground states, the physical underpinnings of the barrier and pathways for slow magnetic relaxation, are less intuitive and may often arise from intermolecular interactions influenced by spin-phonon dynamics.

Previously, we reported the observation of slow magnetic relaxation in some low-spin (S = 1/2) and nearly nuclear spinfree (⁶¹Ni, 1.1% abundant) Ni(III) cyclam complex salts.' We found that nitrate-ligated complexes showed slow magnetic relaxation, while the isothiocyanate-ligated species did not. The slow magnetic dynamics of the Ni(III) compounds appear to be governed by a combination of direct and Raman pathways. Computational studies suggested that the presence of nuclear spin (I) in the axial positions enabled a fast relaxation pathway, undetectable with regular ac magnetometry. We hypothesized that the axial coordination of the nuclear spin-free atoms (16O) has I = 0) is required to observe slow magnetic relaxation in Ni(III) cyclam complexes. While hyperfine coupling is wellknown to quench slow magnetic relaxation with low to no applied field, the quenching effect via superhyperfine coupling in the solid state could offer a unique tool to manipulate the magnetic dynamics of Ni(III) cyclam systems. Overall, the results suggested that alteration of intermolecular interactions

Received: November 15, 2022 Revised: March 10, 2023 Published: March 30, 2023



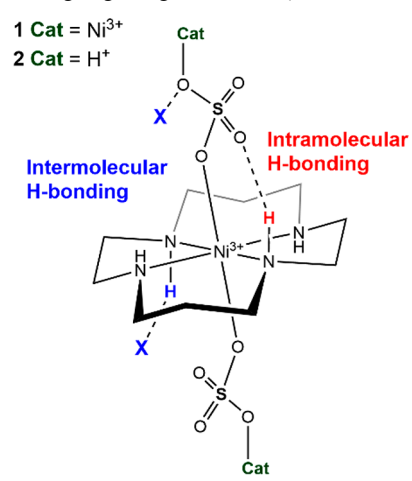


and nuclear spin could serve as synthetically adjustable parameters for control of slow relaxation of magnetization in S = 1/2 systems.

SMM research has focused on understanding the role of vibrations, both intra- and intermolecular (phonons), in recent years.^{20–24} Understanding the roles of connectivity, intermolecular interactions, and phonons is especially important for S = 1/2 systems as they lack the higher magnetic states that are typically considered the barrier toward magnetic relaxation. Furthermore, many S = 1/2 SMMs are affected by the phonon bottleneck effect (PBE), a phenomenon where the phonons emitted by the magnetic relaxation are inefficiently scattered and consequently reabsorbed. 12,25-30 While the PBE increases the spin-lattice relaxation time, a desirable quantity, it is typically considered detrimental as it complicates understanding the molecular relaxation pathways. Notwithstanding, the innate dependence of PBE on the chemical and structural environment may render it a valuable tool in elucidating the importance of different interactions for modulating slow relaxation of magnetization.

To study the effect of intra- and intermolecular interactions on slow magnetic relaxation in Ni(III) cyclam complexes, we targeted several salts that would maintain the magnetically productive N_4O_2 first coordination sphere, change anion geometry relative to previously discussed nitrate complexes, potentially change the overall complex charge to anionic species, and generate more extensive hydrogen bonding networks than the nitrato- and isothiocyanato-bound complexes disclosed previously. Herein, we report the structural and magnetic properties of a sulfate-bridged Ni(III) cyclam chain compound and the first example of bisulfate-bound Ni(III) cyclam complexes (Scheme 1).

Scheme 1. Structural Overview of Polymeric 1 and Molecular 2, Highlighting Chemically Tunable Moieties^a



^aExchangeable protons are shown explicitly. "X" generically refers to the H-bond partner.

■ EXPERIMENTAL SECTION

Unless otherwise noted, compound syntheses and manipulations were performed at room temperature. The precursors $[Ni(cyclam)] \cdot (ClO_4)_2$ and $[Ni(cyclam)Cl_2]Cl$ were synthesized following literature procedures. 31,32 Unless specified, Millipore water was used, and all other reagents were obtained from commercial sources and used without further purification.

 $\{[Ni(cyclam)(SO_4)]CIO_4 \cdot H_2O\}_n$ (1). This compound was synthesized by modifying the literature procedure³³ as follows: cyclam was used in place of tetramethylcyclam (TMC). A 20 mL scintillation vial was charged with solid [Ni(cyclam)](ClO₄)₂ (171 mg, 0.373 mmol) and dissolved in water (10 mL). To the yellow-colored solution, solid Na₂S₂O₈ (48.7 mg, 0.205 mmol) was added all at once and stirred for 30 min, whereupon the product precipitated as a light green powder. Anal. Calcd for C₁₀H₂₆N₄O₉NiS: C, 25.42; H, 5.55; N, 11.86; Found: C, 25.32; H, 5.39; N, 11.71. FT-IR (cm⁻¹) (Figure S2): 3550w, 3415w, 3221w, 3120w, 3044m, 2984w, 2961w, 2936w, 2869m, 2811w, 602m, 565m, 527m. 972m, 944w, 932w, 906m, 891m, 730w, 700w, 630m. Crystals suitable for single crystal X-ray diffraction analysis were synthesized by slowly removing the filtrate under vacuum over the course of 1 week, producing a mixture of dark green blocks of 1 and orange blocks of [Ni(cyclam)](ClO₄)₂.³⁴ The powder diffraction pattern of the green powder 1 was consistent with the calculated pattern of the collected crystal structure (Figure S4).

[Ni(cyclam)(HSO₄)₂]HSO₄·MeOH (2·MeOH). A 20 mL scintillation vial was charged with [Ni(cyclam)Cl₂]Cl (34.9 mg, 0.096 mmol), Ag₂SO₄ (45.5 mg, 0.146 mmol), and a 1:20 MeOH:conc. H₂SO₄ mixture (10 mL). The mixture was stirred for 30 min at room temperature and then filtered to remove the insoluble Ag(I) salts. A vapor diffusion of Et₂O into the MeOH:H₂SO₄ filtrate was performed, but there was no crystal formation after 2 days, whereupon KClO₄ (4.31 mg, 0.031 mmol) was added to the mother liquor to aid crystallization. After 3 days, the mother liquor became biphasic, composed of a green layer and a purple layer, with green and purple crystals coating the side of the vial in their respective layers. Single crystal X-ray diffraction analyses revealed the crystals to be 1 (green) and 2·MeOH (purple). Attempts to isolate 2·MeOH as a pure bulk material were unsuccessful.

[Ni(cyclam)(HSO₄)₂]HSO₄ (2). A flame-dried 25 mL Schlenk flask was charged with [Ni(cyclam)Cl₂]Cl (59.5 mg, 0.163 mmol) and attached to a t-joint connected to a Schlenk line and base bath. The apparatus was flushed with dinitrogen gas, followed by the addition of concentrated sulfuric acid (500 μ L); the mixture was stirred until all solids were dissolved and the solution stopped bubbling (Caution! Produces HCl gas), approximately 10 min. The red/brown solution was diluted with acetonitrile (20 mL), whereupon the solution color turned green, and filtered through a medium-porosity sintered glass frit. The filtrate was transferred to a scintillation vial, capped, and allowed to stand for 2 days at room temperature, whereupon the desired product formed as dark brown needles (29.9 mg, 0.054 mmol, 31%). Anal. Calcd for $C_{10}H_{27}N_4O_{12}NiS_3$: C, 21.83; H, 4.95; N, 10.18; Found: C, 21.97; H, 4.91; N, 10.18. ESI-MS(+) (Figure S8) (m/z): 355.25, [Ni(II)(cyclam)(HSO₄)]⁺; 452.17, [Ni(III)(cyclam)-(HSO₄)₂]⁺. FT-IR (cm⁻¹): 3372sh, 3160m, 3118m, 2864m, 2443w, 2348w, 1688w, 1592w, 1462m, 1453w, 1440m, 1426m, 1385w, 1367w, 1343w, 1335w, 1324w, 1293m, 1265w, 1245m, 1223m, 1208sh, 1157sh, 1142s, 1122sh, 1096sh, 1076sh, 1055sh, 1040sh, 1023s, 940w, 906w, 887s, 867s, 838s, 826sh, 766m, 724m, 604sh, 584sh, 568s, 526sh, 503m, 446m, 428m.

 $[Ni(cyclam-d_4)(DSO_4)_2]DSO_4$ (2-d₇). An apparatus identical with the one described above was prepared and charged with [Ni(cyclam)- Cl_2]Cl (31.6 mg, 0.087 mmol) and concentrated sulfuric acid- d_2 (99% D, 500 μ L). The mixture was stirred until all material was dissolved and the solution stopped bubbling, approximately 10 min. The red solution was diluted with acetonitrile-d₃ (98% D, 2 mL) and filtered through a 0.2 μm nylon filter. The filtrate was transferred to a 1-dram shell vial, capped, and allowed to stand for 2 days at room temperature, whereupon the desired product formed as dark brown needles (15.76 mg, 0.028 mmol, 32%). A powder diffraction pattern and FTIR spectrum were collected to verify bulk purity and extent of deuteration. DART-MS(+) (Figures S9 and S10) (m/z): 230.23, $\begin{aligned} & [\text{Ni}(\text{cyclam-}d_4)(\text{DSO}_4)(\text{D}_2\text{SO}_4)]^{2+}; \ 598.44, \ [\text{Ni}(\text{cyclam-}d_4)(\text{DSO}_4)_2 \\ & + \text{D}_2\text{SO}_4 + \text{D}_2\text{O}]^+; +. \text{FT-IR} \ (\text{cm}^{-1}): \ 3372\text{sh}, \ 3137\text{m}, \ 3105\text{m}, \ 2871\text{m}, \end{aligned}$ 2482m, 2348w, 1688w, 1592w, 1452w, 1436m, 1397w, 1382w, 1367sh, 1342m, 1321m, 1300m, 1267w, 1250 sh, 1235sh, 1218m, 1164sh, 1146s, 1122sh, 1094sh, 1068sh, 1015s, 940w, 906w, 879sh,

857s, 838s, 826sh, 766m, 736m, 604sh, 584sh, 564s, 526sh, 503m, 452m, 433m, 405w.

X-ray Structure Determinations. Crystals suitable for singlecrystal X-ray analysis were coated with Paratone-N oil and supported on a Cryoloop before being mounted on a Bruker Kappa Apex II CCD diffractometer under a stream of dinitrogen. Data collections were performed at low temperature (100-200 K; see Table S1) using a Siemens KFF Mo₂K-90 sealed tube (Mo K α , λ = 0.71073 Å) X-ray source and a curved graphite monochromator, targeting complete coverage and 4-fold redundancy. Crystallographic data and metric parameters are presented in Table S1. Determination of unit cell parameters through refinement, data collection, reduction, and correction for Lorentz and polarization effects was performed using the SAINT software package.³⁵ Data were sorted, scaled, averaged, and corrected for semiempirical absorption affects with SADABS. The structures were solved with the ShelXT structure solution program and refined with the ShelXL-2018/3 refinement package.³ Unless otherwise noted, thermal parameters for all non-hydrogen atoms were refined anisotropically. Hydrogen atoms were added at calculated positions and were refined using a riding model. In the structure of 1, the data were modeled as a two-component pseudomerohedral twin; the refined fractional contribution of the minor component refined to 18%. In the structures of 2 and $2-d_7$, the outer-sphere bisulfate H atoms were found in the electron density difference maps, and DFIX and DANG restraints were used to restrain them to chemically reasonable positions. In the structure of 2. MeOH, the data were modeled as a two-component inversion twin and the refined fractional contribution of the minor component was refined to 44%. Hirshfeld surface analyses were performed for all structures discussed here, and the results are shown in Figures S32-

Magnetic Measurements. Magnetic susceptibility data were collected using a Quantum Design MPMS XL magnetometer for 1 and a Quantum Design MPMS3 magnetometer for 2 and 2-d₇. Samples were ground using a mortar and pestle and selected for different crystallite sizes by passing through size exclusion filters. Three crystallite size regimes were investigated, (a) "crystalline" is ascrystallized polycrystalline (particle size >206 μ m); (b) "ground" is lightly ground (106 μ m < x < 206 μ m); (c) "100 μ m" is heavily ground (53 μ m < x < 106 μ m). The sifted samples were loaded into polyethylene bags and sealed; then, the bags were inserted into drinking straws and inserted into the instrument. Ferromagnetic impurities were checked through a variable field analysis (0 to 10 kOe) of the magnetization at 100 K: overall linearity in the collected data for all three compounds indicated the lack of significant ferromagnetic impurities. Static (dc) magnetic susceptibility data for "ground" samples were collected at temperatures ranging from 3 to 300 K at 1 kOe measuring field (see the Supporting Information for other particle sizes). Alternating current (ac) magnetic susceptibility measurements were performed from 0.1 to 700 Hz and from 1.8 to 15 K with an alternating field of 4 Oe. Data were corrected for the magnetization of the sample holder by subtracting the susceptibility of an empty container and for the diamagnetic contributions of the sample by using Pascal's constants.³⁸

Temperature-dependent magnetic susceptibility data for 1 were modeled using a combination of a Bonner–Fisher component, $^{39-41}$ which modeled the susceptibility of an S=1/2 infinite isotropic Heisenberg chain, and a Curie–Weiss-like component that modeled finite chain lengths with an odd number of Ni^{3+} spins, isolated Ni^{3+} spins, and/or other paramagnetic impurities. The resulting exchange coupling is reported using $H=-S\cdot J\cdot S$ spin Hamiltonian formalism. See the Supporting Information for details.

Temperature-dependent dc magnetic susceptibility data for 2 and 2-d, were modeled with the program PHI⁴² to single-ion species with temperature independent paramagnetism, weakly interacting with the spin bath. See the Supporting Information for details.

The ac magnetic susceptibility data for several particle size-selected samples of $\mathbf{2}$ and $\mathbf{2}$ - \mathbf{d}_7 were fit to several multicomponent relaxation models. Using eq 1, the variables A, B, and n were allowed to refine freely.

$$\tau^{-1} = AT + BT^{n} + \tau_{0}e^{-U_{\text{eff}}/k_{B}T}$$
 (1)

Here, the AT term represents the direct pathways, BT^n , the Raman pathways, and $\tau_0 \exp(-U_{\rm eff}/k_{\rm B}T)$, the Orbach pathway. Several models and temperature ranges were compared (Table S5 and Figures S28–S29), and further details can be found in the Supporting Information.

Other Physical Characterizations. Mass spectrometry experiments were performed on a Thermo-Finnigan LTQ LC/MS-MS ESI-MS instrument, where the sample was introduced via direct infusion using a syringe pump (rate $10 \mu L/s$). The samples were dissolved in Millipore water, methanol, or acetonitrile at a concentration of 0.01 mg/mL. Electronic absorption (UV-visible) spectra (Figure S13) were obtained using quartz cuvettes in an Agilent 8453 spectrometer. Complexes were dissolved in Millipore water. Diffuse reflectance data were obtained with a Thermo Scientific Evolution 300 UV-vis spectrophotometer, using BaSO₄ for background. Infrared spectra were obtained using a Bruker Tensor II FT-IR spectrometer. Electron paramagnetic resonance spectra were obtained using a Bruker ELEXSYS-II E500 CW-EPR spectrometer equipped with an X-band microwave source, an high sensitivity resonator (ER 4122 SHQE Resonator), and a liquid He cryostat with a quartz finger dewar (ESR900 equipped with ColdEdge Stinger). Data were collected with a 5 G modulation amplitude and 100 kHz frequency and were simulated using the software package Easy Spin. 43 Thermal gravimetric analysis (TGA) was performed on a TA Q500 Thermogravimetric Analyzer under a N₂ flow at a rate of 5 °C/min from room temperature to 100 and 10 °C/min thereafter. Powder Xray diffraction data were collected at room temperature using a Scintag X-2 powder X-ray diffractometer equipped with Cu K α radiation, a Peltier detector, and a stationary sample stage, collecting diffraction angles between 5° and 30° 2θ . Elemental analyses were performed by Midwest Microlabs, Indianapolis, IN.

■ RESULTS AND DISCUSSION

Syntheses and Structures. To study the effect of intraand intermolecular interactions on slow magnetic relaxation in Ni(III) cyclam complexes, we synthesized several salts where the axial ligands contained tetrahedral SO₄(H) anions. Our initial attempts to synthesize sulfate-ligated Ni(III) cyclam salts through ion exchange reactions resulted in an inseparable mixture of crystalline Ni(cyclam)(SO₄)(ClO₄) (1) and $[Ni(cyclam)(HSO_4)_2]HSO_4 \cdot MeOH$ (2·MeOH). We note that the nickel sulfate perchlorate compound has been synthesized previously but not characterized crystallographically or had its temperature-dependent magnetic susceptibility characterized, while 2. MeOH represents a first example of a Ni(III) cyclam species bound by bisulfate ligands. To isolate pure products, we adapted a previously reported synthesis for [Ni(TMC)SO₄]ClO₄ for cyclam, producing 1 in good yield, and implemented an acid-base reaction, described in the Experimental Section, for synthesizing pure samples of 2. From these procedures, we isolated the chain compound {[Ni- $(\text{cyclam})(\mu_2\text{-SO}_4)]\text{ClO}_4\cdot\text{H}_2\text{O}_n$ (1, Figure 1, left), the bisulfate-ligated complex [Ni(cyclam)(HSO₄)₂]HSO₄ (2, Figure 1, right), and its deuterated isotopologue $2-d_7$.

Crystallographic analyses (Figure 1 and Supporting Information) show that all four structures feature Ni(III) ions with comparable distorted octahedral coordination geometries. The sulfate-bridged chain featured in 1 is structurally comparable to a Mn-containing compound reported previously by Sessoli and co-workers. The intrachain Ni(III) centers are canted by 11.30(3)° and separated by 6.280(1) Å, whereas the shortest interchain Ni–Ni distance is 8.536(1) Å. In comparison, the Mn analogue is canted by 15.6°; the closest intrachain Mn–Mn distance is 6.362 Å, and the closest interchain Mn–Mn distance is 8.552 Å. Compound 2

Crystal Growth & Design pubs.acs.org/crystal Article

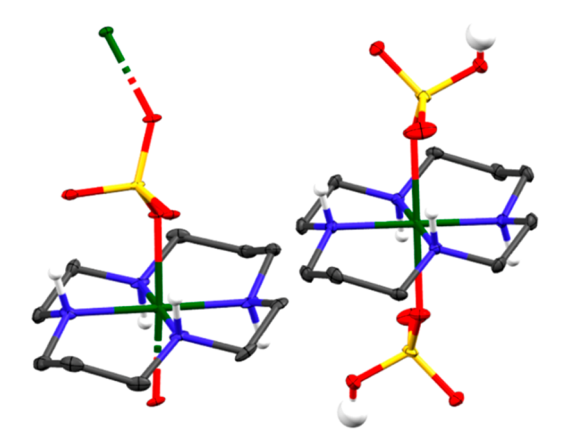


Figure 1. Crystal structures of Ni(III) cyclam complex units in sulfate-bridged chain 1 (left) and bisulfate-ligated molecular 2 (right) rendered with 50% thermal ellipsoids. Green, red, blue, yellow, and gray ellipsoids represent Ni, O, N, S, and C atoms, respectively, and white spheres represent H atoms involved in hydrogen bonding interactions. Solvent molecules, outer sphere anions, and H atoms not involved in hydrogen bonding are omitted for clarity.

represents the first report of a Ni-bisulfate-ligated species, with a Ni-O distance of 2.1135(16) Å. The closest Ni-Ni distance is 7.838(2) Å.

Both 1 and 2 have different anion geometries and generate more extensive hydrogen bonding networks than the nitrato-and isothiocyanato-bound complexes disclosed previously. ^{7,45} Meanwhile, although 2 and 2·MeOH have different hydrogen bonding networks while maintaining similar molecular environments, making them an ideal system to study the effect of hydrogen bonding, we were unable to convert 2 into 2·MeOH without reducing Ni(III) to Ni(II), and as a result, we were unable to isolate pure bulk samples of 2·MeOH for magnetic studies.

Hydrogen bonding in the structure of 1 is localized to each chain with no interchain H-bonding. Each sulfate in 1 makes three hydrogen bonds with the cyclam amines, with N···O distances of 2.82(7), 2.86(6), and 3.06(5) Å. The sulfate is also H-bonded to a cocrystallized H₂O molecule, 2.76(5) Å, which in turn is H-bonded to one outer-sphere perchlorate anion, 2.86(9) Å. In contrast, the structure of 2 features a more extensive network of hydrogen bonding interactions (Figure 2). The intramolecular N-H···OSO₃H distance in 2 is 2.878(2) Å and occurs once for each axial bisulfate moiety, which is also H-bonded to the outer-sphere bisulfate anion with a donor-acceptor distance of 2.521(3) Å. The two remaining amines H-bond to two other outer-sphere bisulfates with distances of 2.829(3) and 2.948(3) Å. The ligated HSO₄ anions in 2 also have a H-bond with another outer-sphere HSO_4^- , with a separation of only 2.466(4) Å. These interactions result in an extensive H-bonding network in 2.

The solid-state structure of the deuterated isotopologue $2 \cdot d_7$ was also determined through X-ray crystallography. It is isostructural with the protiated **2**, showing little change in the bond distances and crystal parameters. A powder diffraction of the material also shows little difference between isotopologues (Figure 3), indicating the lack of isotopic polymorphism. The Hirshfeld surface analysis of **2** and **2**- d_7 and their corresponding fingerprint plots (Figures S34–S35) are different, however. Specifically, the spikes corresponding to the O–H hydrogen bonds are sharp and symmetrical in **2** but more rounded and asymmetrical in **2**- d_7 . These differences may arise

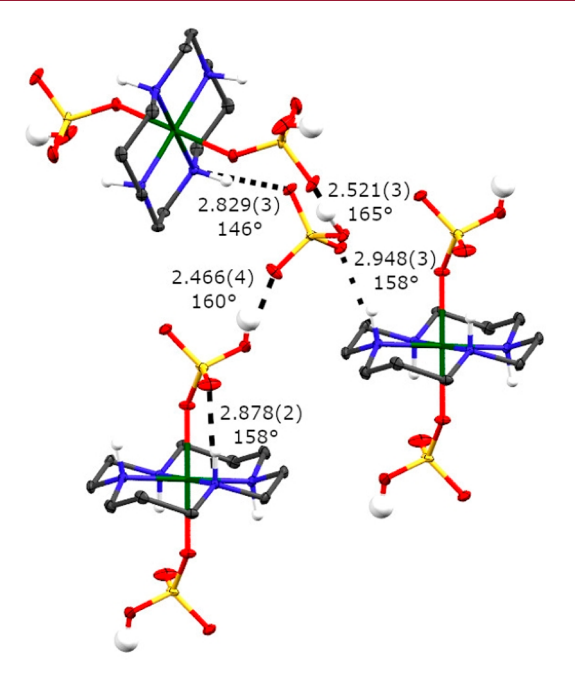


Figure 2. Unique hydrogen bonds in 2 given in Å; angles represent the donor—H-acceptor bond angle. Atom colors are as described in Figure 1. The outer sphere bisulfate moiety is disordered on an inversion center, and only one position is shown for clarity.

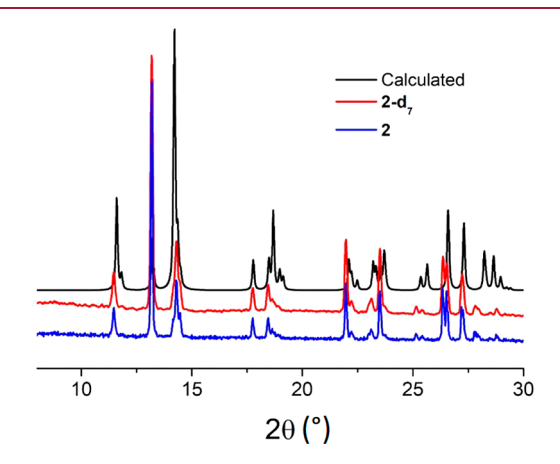


Figure 3. Powder XRD of a ground sample of 2 and 2- d_7 . The calculated trace is derived from single crystal data collected on 2.

from different placement of the H/D atoms in the structures; however, the analysis is obscured by differences and limitations in locating the atoms in difference maps; see the Supporting Information for details.

The IR spectra of 2 and 2- d_7 clearly show shifts in the bands involving the exchangeable protons (Figure 4), and the MS spectra confirm the d_7 assignment (Figures S9 and S10).

We note that the MS spectrum for 2, which used a liquid chromatographic introduction system, shows peaks consistent with Ni(II) and Ni(III) species, whereas the solid-state introduction system (DART) used for analyzing 2-d₇ only shows Ni(III) species. We attribute this difference to an artifact of the data collection method. Nevertheless, this highlights the importance of the proton inventory for the stability of the Ni(III) oxidation state, where the solution-phase introduction system is more likely than the solid-state introduction system to deprotonate the amines and initiate the reduction process. $^{46-49}$

Crystal Growth & Design pubs.acs.org/crystal Article

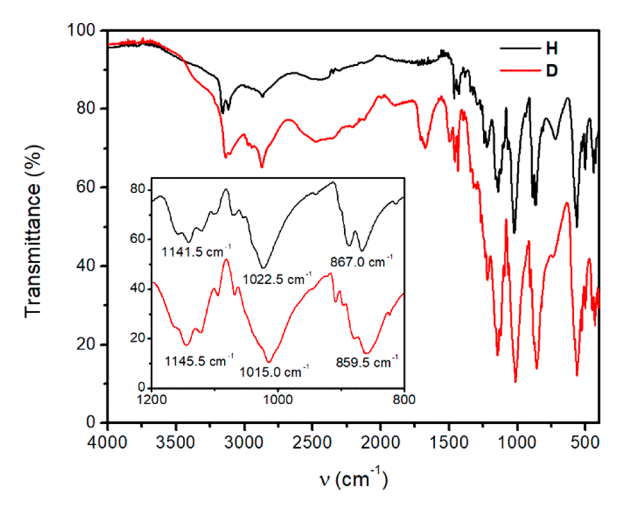


Figure 4. FTIR spectrum of 2 and $2-d_7$ from 4000 to 400 cm⁻¹. Inset corresponds to characteristic bisulfate bands shifted by deuteration.

The structure of solvatomorph **2·MeOH** is like **2** in several ways; however, the addition of methanolic H-bonds changes the symmetry significantly. The intramolecular N–H···OSO₃H distance is 2.878(8) Å for the bisulfate anion near the MeOH and 2.823(8) Å for the other. The two remaining amines H-bond to the outer-sphere bisulfates with donor—acceptor distances of 2.799(7) and 3.007(8) Å, respectively. The innersphere bisulfate interacts with both the outer-sphere bisulfate, with distances of 2.625(8) and 2.888(8) Å, and the methanol solvate at 2.552(8) Å. Methanol also hydrogen bonds to the outer-sphere HSO_4^- at 2.70(1) Å. While **2** has shorter (and presumably stronger) H-bonds stronger than the **2·MeOH** solvatomorph, the reduction in symmetry results in a greater number of unique H-bonds for **2·MeOH**, which in principle could influence magnetic relaxation properties.

Static (dc) Magnetic Properties. The temperature dependencies of the magnetic susceptibility-temperature products ($\chi_{\rm M}T$) of ground samples of 1 and 2, collected between 2 and 300 K with an applied dc field of 1000 Oe (Figure 5), show that both complexes possess S=1/2 Ni(III) ions, but interact with neighbors differently. The coordination polymer 1 shows a $\chi_{\rm M}T$ value of 0.43 cm³ K mol⁻¹ at 300 K. Upon cooling, the magnetic susceptibility product decreases gradually at first and then more rapidly below 75 K, to a

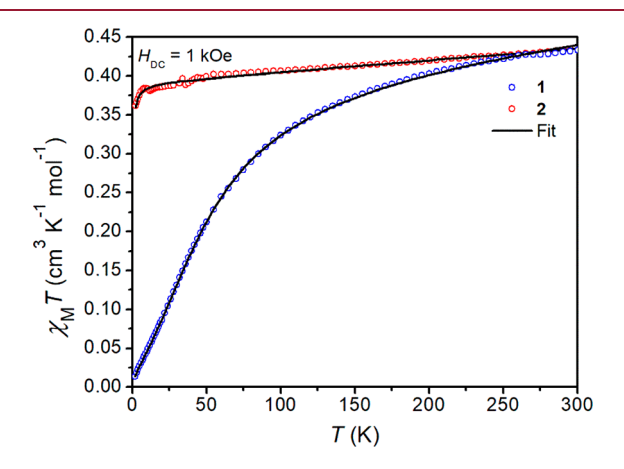


Figure 5. Static (DC) magnetic susceptibility of ground samples of 1 and 2 in a 1 kOe applied field from 1.8 to 300 K. Fits are described in the Supporting Information.

minimum of 0.014 cm³ K mol⁻¹ at 2 K, consistent with an antiferromagnetic coupling within chains. The molecular bisulfate complex 2 displays a room temperature $\chi_{\rm M}T$ value of 0.43 cm³ K mol⁻¹. Upon cooling, the $\chi_{\rm M}T$ value decreases gradually until reaching 0.402 cm³ K mol⁻¹ at 55 K, below which there is a pronounced downturn reaching a minimum of 0.36 cm³ K mol⁻¹ at 2 K.

The susceptibility data for 1 are fit to a combination of the Bonner–Fisher model for chain compounds, a Curie–Weisslike model, and a temperature-independent paramagnetism (χ_{TIP}) parameter (see the Supporting Information for details). The fit for 1 yields g=2.20, consistent with the value obtained via EPR ($g_{x,y}=2.24$, $g_z=2.04$; see the Supporting Information). The strength of the antiferromagnetic coupling (-46.3 cm^{-1}) is much higher than that found for the Mn analogue measured by Sessoli and co-workers (-2.9 cm^{-1}), ⁴⁴ but that is consistent with other literature examples where the metal ions have lower spin. ⁵⁰ A similar Cr dimer complex, [Cr(cyclam)(μ -SO₄)₂Cr(cyclam)](ClO₄)₂ similarly showed weak antiferromagnetic coupling, with $J=(-)4.7 \text{ cm}^{-1}$, and a Co(II) dimer complex [Co₂(DMIM)₄(SO₄)₂] (DMIM = 1,2-dimethylimidazole) showed intermediate antiferromagnetic coupling with $J=(-)28 \text{ cm}^{-1}$. ^{51,52}

The plots of temperature dependence of $\chi_{\rm M}T$ (Figure 5) and reduced field magnetization (Figure S17) support the S=1/2 ground state for **2**. The susceptibility data were fit⁴² to determine g, the mean-field intermolecular interaction zJ, and the contributions from $\chi_{\rm TIP}$. The fit for **2** yielded a slightly lower g value (g=2.04) than the EPR ($g_x=2.23$, $g_y=2.14$, $g_z=2.09$) but is still within reasonable agreement.

Dynamic (ac) Magnetic Properties. Dynamic magnetic properties were probed for 1 and 2. Unsurprisingly, 1 shows no in-phase or out-of-phase ac susceptibility, owing to an overall singlet ground state arising from antiferromagnetic coupling of Ni(III) ions through sulfate and hydrogen-bonding networks. In contrast, bisulfate-bound 2 shows slow magnetic relaxation in an applied dc field, which is qualitatively distinct from the behavior previously reported for [Ni(cyclam)(NO₃)₂]^{+,7} The field dependence of the ac susceptibility was studied for 2 at 2 K (Figure S20). Bisulfate-ligated 2 shows a multimode relaxation profile, in contrast to the nitrate species. At low applied dc field, 1 kOe, only a single peak can be observed in the out-of-phase data, with a maximum susceptibility at 150 Hz. Increasing the applied dc field suppresses this highfrequency relaxation pathway, and a new low-frequency pathway centered at 1 Hz emerges at 6 kOe. The temperature dependence of the ac susceptibility was further investigated for 2 under a 6 kOe applied dc field (Figure S22), and it shows the peak in the out-of-phase signal rapidly moving to higher frequencies up to 4 K, whereupon the increase with temperature slows substantially.

In an effort to deconvolute intra- and intermolecular contributions to the observed slow relaxation, we focus here on structural aspects of **2** that can be tuned synthetically and measurement ranges where magnetic events can be captured as fully as possible. Particle size selection and deuteration represent distinct ways to alter intermolecular interactions while minimizing changes to the local ligand field environment of Ni(III) ions. Our inspirations for the deuteration studies come from an example in solution-phase pulsed EPR spectroscopy where deuteration led to increased decoherence times for a V(IV) complex, ¹⁹ and a solid-state magnetic study on a Co(II) complex where deuteration was claimed to quench

Crystal Growth & Design pubs.acs.org/crystal Article

PBE and slow down molecular relaxation processes. To study a magnetic relaxation event over a larger temperature and applied field regime and because slower relaxations are more desirable in qubits, we focused our investigations on the low-frequency pathway identified above. From the temperature dependence data, the peak locations of the out-of-phase $\chi''(\nu)$ maxima were found, and the relaxation times, τ , were extracted and plotted using logarithmic values. These data for several samples of 2 are collected in Figure 6, acquired under the conditions favoring the original low-frequency event.

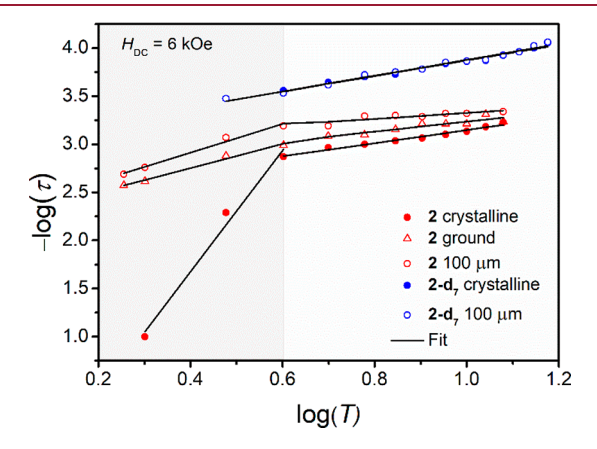


Figure 6. Crystallite size dependence of relaxation rates for several size-selected samples of **2** and **2-d**₇, as measured under a static dc field of 6 kOe. Size-selected samples of **2**: as-crystallized (**2 crystalline**, $x > 206 \mu \text{m}$), lightly ground (**2 ground**, $106 \mu \text{m} < x < 206 \mu \text{m}$), and more finely ground (**2 100 \mu \text{m}**, 53 $\mu \text{m} < x < 106 \mu \text{m}$). Best fit lines are fit from the log–log data to the equation $-\log(\tau) = n \times \log(T) + b$, where $b = 10^C$.

For protiated samples of 2, we identify two temperature-based regimes, <4 K and >4 K, where significant changes occur in the relaxation. The effect is most pronounced for the sample with the largest particle size (2 crystalline, $x > 206 \ \mu m$) but is also observed for the samples with smaller particle sizes (2 ground, $106 \ \mu m < x < 206 \ \mu m$; 2 $100 \ \mu m$, 53 $\mu m < x < 106 \ \mu m$). Interestingly, the deuterated analogues 2-d₇ 100 crystalline and 2-d₇ 100 μm do not show differences in temperature dependence of relaxation times based on particle size.

Extracting magnetic relaxation mechanisms from the plots in Figure 6, we acknowledge that multiple pathways exist in 2 and can be accessed or suppressed under different environmental conditions. Notwithstanding, for self-consistency in the analysis, we treat the relaxation data and fits as if there is only one event to be modeled and separate all samples into the two temperature ranges relevant to 2 crystalline; thus, fitted parameters presented in Table 1 should be regarded provisionally.

In principle, when plotted as a double log plot, the slope of the line corresponds to the exponent of the temperature dependence for scenarios where one relaxation pathway is dominant. Building from eq 1, for a system with only the direct relaxation pathway operative, we would expect a linear temperature dependence, corresponding to a slope of n = 1, whereas for a system where the phonon bottleneck is operative, we would expect a temperature dependence of T^2 and a slope of n = 2, and Raman relaxation processes are often marked by larger slopes (n > 2). In systems with multiple relaxation

Table 1. Relaxation Parameters for 2 and 2-d $_7$ at Different Particle Sizes

$B (s^{-1} T^{-n})$	n
0.143	6.3
292.415	0.68
179.102	1.25
516.654	0.52
207.682	1.49
1027.596	0.32
1148.682	0.81
1136.842	0.82
	0.143 292.415 179.102 516.654 207.682 1027.596 1148.682

pathways, we expect an n value between the pure systems and a slight deviation from linearity. For a S=1/2 system without spin—orbit coupling, as evidenced by the dc magnetic measurements, an Orbach relaxation pathway is not realistic as there are only two available magnetic states, $m_s=+1/2$ and $m_s=-1/2$. As a result, the Orbach term was discarded (see the Supporting Information for fits to alternative models). Instead, only the Raman term was used in the final fits as the data in the log—log plots of relaxation times vs temperature gave nearly linear fits when constrained to the two temperature regimes.

We find interesting particle size-dependent relaxation dynamics for compound 2 both below and above 4 K. The as-crystallized sample (2 crystallized) shows a Raman-like temperature dependence below 4 K (n = 6.3) and a temperature dependence roughly consistent with a direct pathway at higher temperatures. For the lightly ground sample of (2 ground), the parameter n = 1.25 suggests a combination of direct and phonon bottleneck (PB) relaxation pathways at low temperatures. Above 4 K, the *n* parameter dops to 0.52, significantly lower than what is normally expected for Raman or direct processes. The 100 μ m size-selected sample similarly shows behavior provisionally interpreted as a combination of PB and direct processes at low temperature, with a switch to an anomalously slow pathway above 4 K. Of the three samples, the largest and smallest particle sizes show significant changes in slope at 4 K, while the 2 ground sample has a more gradual change with temperature. Meanwhile, the isostructural deuterated analogues 2-d₇ crystalline and 2-d₇ 100 μ m show essentially the same temperature dependencies, with fitted nvalues suggesting a direct relaxation pathway, similar to 2 100 μ m. The particle size dependence seems to have disappeared upon deuteration, from which we could infer that deuteration somehow quenches the PBE, leaving only the faster, molecular relaxation pathways.

Whereas the anomalous values of n extracted from the data do not enable unambiguous identification of PBE pathways, other chemical tuning can reveal those intermolecular effects. Assignment of the PBE is often supported by examining magnetic dilution with an analogous diamagnetic species, where relaxation rates should increase as the magnetic species becomes more dilute.7 Unfortunately, we were unable to replace Ni(III) with diamagnetic ions Co(III), Al(III), or Ti(III) due to synthetic difficulties. Alternatively, studies by Sessoli, Mosser, and Yamashita have shown that the relaxation rate of PB increases with decreasing crystallite size as the increased surface area results in increased phonon scattering, hindering the bottleneck. 25,54,55 Relaxation profiles, collected in Figure 7 at one temperature and applied dc field, illustrate the increased rate of relaxation upon particle size reduction, at least for the protiated samples.

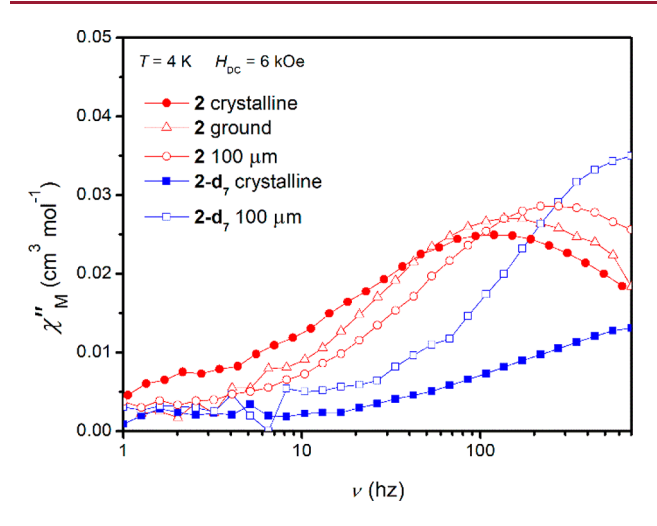


Figure 7. Particle size influences frequency dependence of out-of-phase magnetic susceptibilities of various forms of the bisulfate-containing **2**: crystalline, ground crystalline, and $100 \mu m$ sample of **2** and $2 \cdot d_7$, measured with a 6 kOe applied field at 4 K. Normalized data showing $2 \cdot d_7$ sample overlap are provided in Figure S31.

Both 2 ground and 2 100 µm samples show higher frequency relaxation events than the 2 crystalline sample, consistent with the presence of a phonon bottleneck-like effect. Interestingly, the relaxation event moves to even higher frequencies when the isotopologues are interrogated. We note that slower relaxation upon deuteration was observed by Song and co-workers for a structurally similar Co(II) complex,⁵³ and will discuss this in more detail below. We also note a large increase in the out-of-phase susceptibility value is observed after 2-d₇ crystalline is ground to produce 2d₇ 100 μm, suggesting that a larger proportion of magnetic units are undergoing slow magnetic relaxation in the ground sample. This same effect is observed for the protiated analogues, albeit more subtly within the same particle size regime. Elucidating the origins of this effect require further investigation. The observation is not consistent with PBE, because larger crystals are less likely to scatter the phonons responsible for relaxation, and that would lead to a larger signal. Instead, we speculate that intramolecular relaxation pathways are being revealed by the production of smaller particle sizes.

Although precise pathways for magnetic relaxation cannot be fully separated for 2, we find that both particle size and deuteration clearly influence the dynamic magnetic properties, and these effects can be traced back to the hydrogen bonding network connecting [Ni(cyclam)(HSO₄)₂]⁺ complexes. Deuteration-induced changes in H-bond strength have been studied in a wide variety of compounds with varying results. In some systems, such as oxalic acid dihydrate, deuteration changes Hbond strength by lengthening the donor-acceptor distance, whereas H-bonds involving deuterated phenol are generally stronger than the isotopologue, without structural changes. 56,5 For crystal structures of compound 2, non-H/D atoms do not move upon deuteration, so any changes to bond strength would be related provisionally to dispersion. Regardless of the origin, we do know that the phonon energetics are changed by reference to the FT-IR spectra shown in Figure 4. The complexity of H/D-bond strength changes is especially relevant in 2, as there are two general types of H-bonds: (1) between bisulfates and (2) between the cyclam amines and

inner- and outer-sphere bisulfates. In contrast, in the study reported by Song and co-workers, where deuteration of a Co(II) complex led to slower relaxation, the deuteration was localized to a ligated acetonitrile molecule, which did not participate in H-bonding. Additionally, exchanging H for D also changes the nuclear spin on those sites from I=1/2 to I=1, which has been shown in pulsed EPR experiments to affect T_1 . Given the proximity of the spin changes to the Ni(III) center and the complexity of the H-bonding framework, it perhaps should be expected that the relaxation dynamics of 2 would change drastically upon deuteration.

CONCLUSIONS

Overall, we report the magnetic relaxation dynamics of two Ni(III) salts of comparable first coordination spheres. Consistent with our predictions from our previous report, $[Ni(cyclam)(HSO_4)_2]^+$ in 2 exhibits slow magnetic relaxation with axially coordinated oxygen atoms, whereas the antiferromagnetism in 1 precludes magnetic relaxation as a singlet ground state does not possess any magnetic moment available for relaxation. The magnetic dynamic measurements exhibit the presence of multiple relaxation pathways, the faster of which is quenched by applying a stronger magnetic field. The slower pathway is assigned as a mixture of Raman, PB, and direct pathways, where the relative contributions vary significantly with particle size and temperature regime. Deuteration of 2 reveals a faster relaxation pathway that does not change with particle size. We believe that, by deuterating 2, we quench the phonon bottleneck effect through altering the energetics of the H-bonding network. While isotopic influences on the phonon landscape are complicated and system dependent, the observation of significant magnetic dynamic changes upon deuteration suggests that further investigation of isotope effects on magnetostructural properties will be useful for the broader magnetism community and could serve as a synthetic tool for modulating magnetic frameworks.

ASSOCIATED CONTENT

Supporting Information

The Supporting Information is available free of charge at https://pubs.acs.org/doi/10.1021/acs.cgd.2c01347.

Tables of select bond distances, mass spectrometry, and other characterization data for 1, 2, and 2- d_7 ; additional magnetic data and details of magnetic property interpretation for the same compounds (PDF)

Accession Codes

CCDC 2216212–2216215 contain the supplementary crystallographic data for this paper. These data can be obtained free of charge via www.ccdc.cam.ac.uk/data_request/cif, or by emailing data_request/cif, or by contacting The Cambridge Crystallographic Data Centre, 12 Union Road, Cambridge CB2 1EZ, UK; fax: +44 1223 336033.

AUTHOR INFORMATION

Corresponding Author

Matthew P. Shores — Department of Chemistry, Colorado State University, Fort Collins, Colorado 80523-1872, United States; orcid.org/0000-0002-9751-0490; Email: matthew.shores@colostate.edu

Authors

Thomas L. Morrison – Department of Chemistry, Colorado State University, Fort Collins, Colorado 80523-1872, United States

Indrani Bhowmick — Department of Chemistry and Analytical Resources Core, Colorado State University, Fort Collins, Colorado 80523-1872, United States

Complete contact information is available at: https://pubs.acs.org/10.1021/acs.cgd.2c01347

Author Contributions

T.L.M. synthesized and measured all compounds. I.B. assisted with data analysis. M.P.S. assisted with visualization, conceptualization, methodology, and writing. The manuscript was written through contributions of all authors. All authors have given approval to the final version of the manuscript.

Notes

The authors declare no competing financial interest.

ACKNOWLEDGMENTS

This work was supported by National Science Foundation, CHE-1800554 and 1956399, and the NIH Shared Instrumentation Grant (SIG) 1S10OD021814-01. The authors thank Prof. Melissa Reynolds for access to and assistance with diffuse reflectance measurements. The authors also wish to thank the Analytical Resources Core (RRID: SCR_021758) at Colorado State University for instrument access, training, and assistance with sample analysis. We thank Dr. Brian Newell for assistance with Hirshfield analyses.

REFERENCES

- (1) Martínez-Pérez, M. J.; Cardona-Serra, S.; Schlegel, C.; Moro, F.; Alonso, P. J.; Prima-García, H.; Clemente-Juan, J. M.; Evangelisti, M.; Gaita-Ariño, A.; Sesé, J.; Van Slageren, J.; Coronado, E.; Luis, F. Gd-Based Single-Ion Magnets with Tunable Magnetic Anisotropy: Molecular Design of Spin Qubits. *Phys. Rev. Lett.* **2012**, *108* (24), 1–5.
- (2) Brunet, G.; Safin, D. A.; Jover, J.; Ruiz, E.; Murugesu, M. Single-Molecule Magnetism Arising from Cobalt(II) Nodes of a Crystalline Sponge. *J. Mater. Chem. C* **2017**, *5* (4), 835–841.
- (3) Mannini, M.; Pineider, F.; Sainctavit, P.; Danieli, C.; Otero, E.; Sciancalepore, C.; Talarico, A. M.; Arrio, M. A.; Cornia, A.; Gatteschi, D.; Sessoli, R. Magnetic Memory of a Single-Molecule Quantum Magnet Wired to a Gold Surface. *Nat. Mater.* **2009**, *8* (3), 194–197.
- (4) Aromí, G.; Aguilà, D.; Gamez, P.; Luis, F.; Roubeau, O. Design of Magnetic Coordination Complexes for Quantum Computing. *Chem. Soc. Rev.* **2012**, *41*, 537–546.
- (5) Frost, J. M.; Harriman, K. L. M.; Murugesu, M. The Rise of 3-d Single-Ion Magnets in Molecular Magnetism: Towards Materials from Molecules? *Chem. Sci.* **2016**, *7* (4), 2470–2491.
- (6) Craig, G. A.; Murrie, M. 3D Single-Ion Magnets. *Chem. Soc. Rev.* **2015**, 44 (8), 2135–2147.
- (7) Bhowmick, I.; Roehl, A. J.; Neilson, J. R.; Rappé, A. K.; Shores, M. P. Slow Magnetic Relaxation in Octahedral Low-Spin Ni(III) Complexes. *Chem. Sci.* **2018**, 9 (31), 6564–6571.
- (8) Woodruff, D. N.; Winpenny, R. E. P.; Layfield, R. A. Lanthanide Single-Molecule Magnets. *Chem. Rev.* **2013**, *113* (7), 5110–5148.
- (9) Stinghen, D.; Atzori, M.; Fernandes, C. M.; Ribeiro, R. R.; De Sá, E. L.; Back, D. F.; Giese, S. O. K.; Hughes, D. L.; Nunes, G. G.; Morra, E.; Chiesa, M.; Sessoli, R.; Soares, J. F. A Rare Example of Four-Coordinate Nonoxido Vanadium(IV) Alkoxide in the Solid State: Structure, Spectroscopy, and Magnetization Dynamics. *Inorg. Chem.* **2018**, *57* (18), 11393–11403.
- (10) Tesi, L.; Lucaccini, E.; Cimatti, I.; Perfetti, M.; Mannini, M.; Atzori, M.; Morra, E.; Chiesa, M.; Caneschi, A.; Sorace, L.; Sessoli, R.

- Quantum Coherence in a Processable Vanadyl Complex: New Tools for the Search of Molecular Spin Qubits. *Chem. Sci.* **2016**, 7 (3), 2074–2083.
- (11) Albino, A.; Benci, S.; Tesi, L.; Atzori, M.; Torre, R.; Sanvito, S.; Sessoli, R.; Lunghi, A. First-Principles Investigation of Spin-Phonon Coupling in Vanadium-Based Molecular Spin Quantum Bits. *Inorg. Chem.* **2019**, *58* (15), 10260–10268.
- (12) Ding, M.; Cutsail, G. E.; Aravena, D.; Amoza, M.; Rouzières, M.; Dechambenoit, P.; Losovyj, Y.; Pink, M.; Ruiz, E.; Clérac, R.; Smith, J. M. A Low Spin Manganese(IV) Nitride Single Molecule Magnet. *Chem. Sci.* **2016**, *7* (9), 6132–6140.
- (13) Cui, H. H.; Sun, T. M.; Wang, M.; Chen, L.; Tang, Y. F. Bulky Anion Supported a Five-Coordinate Spin-Crossover Cobalt(II) Complex with Slow Magnetic Relaxation. *J. Solid State Chem.* **2020**, 289 (June), 121535.
- (14) Chen, L.; Song, J.; Zhao, W.; Yi, G.; Zhou, Z.; Yuan, A.; Song, Y.; Wang, Z.; Ouyang, Z. W. A Mononuclear Five-Coordinate Co(II) Single Molecule Magnet with a Spin Crossover between the S=1/2 and 3/2 States. *Dalt. Trans.* **2018**, 47 (46), 16596–16602.
- (15) Bhowmick, I.; Shaffer, D. W.; Yang, J. Y.; Shores, M. P. Single Molecule Magnet Behaviour in a Square Planar: S=1/2 Co(II) Complex and Spin-State Assignment of Multiple Relaxation Modes. *Chem. Commun.* **2020**, *56* (49), *6711*–*6714*.
- (16) Lin, W.; Bodenstein, T.; Mereacre, V.; Fink, K.; Eichhöfer, A. Field-Induced Slow Magnetic Relaxation in the Ni(I) Complexes $[NiCl(PPh_3)_2] \cdot C_4H_8O$ and $[Ni(N(SiMe_3)_2)(PPh_3)_2]$. *Inorg. Chem.* **2016**, 55 (5), 2091–2100.
- (17) Boča, R.; Rajnák, C.; Titiš, J.; Valigura, D. Field Supported Slow Magnetic Relaxation in a Mononuclear Cu(II) Complex. *Inorg. Chem.* **2017**, *56* (3), 1478–1482.
- (18) Cui, H. H.; Lv, W.; Tong, W.; Chen, X. T.; Xue, Z. L. Slow Magnetic Relaxation in a Mononuclear Five-Coordinate Cu(II) Complex. Eur. J. Inorg. Chem. 2019, 2019 (43), 4653–4659.
- (19) Yu, C. J.; Graham, M. J.; Zadrozny, J. M.; Niklas, J.; Krzyaniak, M. D.; Wasielewski, M. R.; Poluektov, O. G.; Freedman, D. E. Long Coherence Times in Nuclear Spin-Free Vanadyl Qubits. *J. Am. Chem. Soc.* **2016**, 138 (44), 14678–14685.
- (20) Cremer, D.; Kraka, E. From Molecular Vibrations to Bonding, Chemical Reactions, and Reaction Mechanism. *Curr. Org. Chem.* **2010**, *14* (15), 1524–1560.
- (21) Gu, L.; Wu, R. Origin of the Anomalously Low Raman Exponents in Single Molecule Magnets. *Phys. Rev. B* **2021**, *103* (1), 1–9.
- (22) Lunghi, A.; Sanvito, S. Spin-Phonon Relaxation in Molecular Qubits from First Principles Spin Dynamics; arXiv, Quantum Physics, 2019, arXiv:1903.01424, https://arxiv.org/abs/1903.01424v1.
- (23) Mautner, F. A.; Bierbaumer, F.; Fischer, R. C.; Tubau, A.; Speed, S.; Ruiz, E.; Massoud, S. S.; Vicente, R.; Gómez-Coca, S. Insights into the Spin Dynamics of Mononuclear Cerium(III) Single-Molecule Magnets. *Inorg. Chem.* **2022**, *61* (29), 11124–11136.
- (24) Escalera-Moreno, L.; Suaud, N.; Gaita-Ariño, A.; Coronado, E. Determining Key Local Vibrations in the Relaxation of Molecular Spin Qubits and Single-Molecule Magnets. *J. Phys. Chem. Lett.* **2017**, 8 (7), 1695–1700.
- (25) Tesi, L.; Lunghi, A.; Atzori, M.; Lucaccini, E.; Sorace, L.; Totti, F.; Sessoli, R. Giant Spin-Phonon Bottleneck Effects in Evaporable Vanadyl-Based Molecules with Long Spin Coherence. *Dalt. Trans.* **2016**, 45 (42), 16635–16643.
- (26) Nash, F. R. Electron Spin Relaxation in Copper Tutton Salts at Low Temperatures. *Phys. Rev.* **1965**, *138* (5A), A1500.
- (27) Bartolomé, E.; Arauzo, A.; Luzón, J.; Melnic, S.; Shova, S.; Prodius, D.; Nlebedim, I. C.; Bartolomé, F.; Bartolomé, J. High Relaxation Barrier in Neodymium Furoate-Based Field-Induced SMMs. *Dalt. Trans.* **2019**, *48* (41), 15386–15396.
- (28) Pedersen, K. S.; Dreiser, J.; Weihe, H.; Sibille, R.; Johannesen, H. V.; Sørensen, M. A.; Nielsen, B. E.; Sigrist, M.; Mutka, H.; Rols, S.; Bendix, J.; Piligkos, S. Design of Single-Molecule Magnets: Insufficiency of the Anisotropy Barrier as the Sole Criterion. *Inorg. Chem.* **2015**, 54 (15), 7600–7606.

- (29) Lopez, N.; Prosvirin, A. V.; Zhao, H.; Wernsdorfer, W.; Dunbar, K. R. Heterospin Single-Molecule Magnets Based on Terbium Ions and TCNQF 4 Radicals: Interplay between Single-Molecule Magnet and Phonon Bottleneck Phenomena Investigated by Dilution Studies. *Chem. A Eur. J.* **2009**, *15* (42), 11390–11400.
- (30) Wu, S. Q.; Miyazaki, Y.; Nakano, M.; Su, S. Q.; Yao, Z. S.; Kou, H. Z.; Sato, O. Slow Magnetic Relaxation in a Mononuclear Ruthenium(III) Complex. *Chem. A Eur. J.* **2017**, 23 (42), 10028–10033.
- (31) Taraszewska, J.; Sadło, J.; Michalik, J.; Korybut-Daszkiewicz, B. Stability and ESR Spectra of Ni(III) Tetraazamacrocyclic Complexes in Nitrate and Chloride Solutions. *Polym. J. Chem.* **2000**, 74 (6), 813–822.
- (32) Barefield, E. K. A New Synthesis of 1,4,8,11-Tetraazacyclote-tradecane (Cyclam) via the Nickel(II) Complex. *Inorg. Chem.* **1972**, 11, 2273–2274.
- (33) Gore, E. S.; Busch, D. H. Stable Octahedral, Low-Spin Nickel(III) Complexes of a Tetradentate Macrocyclic Ligand Having Saturated Nitrogen Donors. *Inorg. Chem.* **1973**, *12* (1), 1–3.
- (34) Prasad, L.; Nyburg, S. C.; McAuley, A. The Structure of Ni(Cyclam)(ClO₄)₂. Acta Crystallogr. **1987**, C43, 1038–1042.
- (35) Bruker AXS Inc. SAINT, v.8.38A; Bruker Analytical X-Ray Systems, Inc.: Madison, WI, 2016.
- (36) Sheldrick, G. M. SADABS, Version 2.03; Bruker Analytical X-Ray Systems, Inc.: Madison, WI, 2000.
- (37) Sheldrick, G. M. Crystal Structure Refinement with SHELXL. Acta Crystallogr. Sect. C Struct. Chem. 2015, 71 (Md), 3-8.
- (38) Bain, G. A.; Berry, J. F. Diamagnetic Corrections and Pascal's Constants. J. Chem. Educ. 2008, 85 (4), 532-536.
- (39) Ami, T.; Crawford, M. K.; Harlow, R. L.; Wang, Z. R.; Johnston, D. C.; Huang, Q.; Erwin, R. W. Magnetic Susceptibility and Low-Temperature Structure of the Linear Chain Cuprate Sr2CuO3. *Phys. Rev. B* **1995**, *51* (9), 5994–6001.
- (40) Bonner, J. C.; Fisher, M. E. Linear Magnetic Chains with Anisotropic Coupling. *Phys. Rev.* **1964**, *135* (3A), A640.
- (41) Duffy, W.; Barr, K. Alternating Antiferromagnetic Heisenberg Linear Chains. J. Appl. Phys. 1968, 39 (2), 969.
- (42) Chilton, N. F.; Anderson, R. P.; Turner, L. D.; Soncini, A.; Murray, K. S. PHI: A Powerful New Program for the Analysis of Anisotropic Monomeric and Exchange-Coupled Polynuclear d- and f-Block Complexes. *J. Comput. Chem.* **2013**, *34* (13), 1164–1175.
- (43) Stoll, S.; Schweiger, A. EasySpin, a Comprehensive Software Package for Spectral Simulation and Analysis in EPR. *J. Magn. Reson.* **2006**, *178* (1), 42–55.
- (44) Mossin, S.; Weihe, H.; Osholm Sørensen, H.; Lima, N.; Sessoli, R. Rationalisation of Weak Ferromagnetism in Manganese(III) Chains: The Relation between Structure and Ordering Phenomena. *J. Chem. Soc. Dalt. Trans.* **2004**, *4* (4), 632–639.
- (45) Yamashita, M.; Toriumi, K.; Ito, T. Structure of Bis-(Isothiocyanato)(1,4,8,1 l-Tetraazacyclotetradecane)Nickel(III) Perchlorate. *Acta* **1985**, *C41*, 1607–1609.
- (46) Bossu, F. P.; Margerum, D. W. The Stabilization of Trivalent Nickel in Deprotonated-Peptide Complexes. *J. Am. Chem. Soc.* **1976**, 98 (13), 4003–4004.
- (47) Zilbermann, I.; Maimon, E.; Cohen, H.; Meyerstein, D. Redox Chemistry of Nickel Complexes in Aqueous Solutions. *Chem. Rev.* **2005**, *105* (6), 2609–2625.
- (48) Shamir, D.; Zilbermann, I.; Maimon, E.; Shames, A. I.; Cohen, H.; Meyerstein, D. Anions as Stabilizing Ligands for Ni(III)(Cyclam) in Aqueous Solutions. *Inorg. Chim. Acta* **2010**, *363* (12), 2819–2823.
- (49) Haines, R. I.; McAuley, A. Synthesis and Reactions of Nickel(III) Complexes. *Coord. Chem. Rev.* **1981**, 39, 77–119.
- (50) Keene, D. T.; Zimmermann, I.; Neels, A.; Sereda, O.; Hauser, J.; Bonin, M.; Hursthouse, B. M.; Price, J. D.; Decurtins, S. Heterocyclic Amine Directed Synthesis of Metal(II)-Oxalates: Investigating the Magnetic Properties of Two Complete Series of Chains with S = 5/2 to S = 1/2. *Dalt. Trans.* **2010**, 39 (20), 4937–4950.

- (51) Glerup, J.; Goodson, P. A.; Hodgson, D. J.; Masood, M. A.; Michelsen, K. Syntheses and Characterization of Novel Binuclear Chromium (III) Complexes of 1,4,8,11-Tetraazacyclotetradecane (Cyclam). *Inorg. Chim. Acta* **2005**, 358 (2), 295–302.
- (52) Murphy, M. J.; Usov, P. M.; Rizzuto, F. J.; Kepert, C. J.; D'Alessandro, D. M. Magnetic, Electrochemical and Optical Properties of a Sulfate-Bridged Co(II) Imidazole Dimer. *New J. Chem.* **2014**, 38 (12), 5856–5860.
- (53) Li, J.; Xiong, S.-J.; Li, C.; Jin, B.; Zhang, Y.-Q.; Jiang, S.-D.; Ouyang, Z.-W.; Wang, Z.; Wu, X.-L.; van Tol, J.; Song, Y. Manipulation of Molecular Qubits by Isotope Effect on Spin Dynamics. *CCS Chem.* **2021**, 3, 2548–2556.
- (54) Petukhov, K.; Bahr, S.; Wernsdorfer, W.; Barra, A. L.; Mosser, V. Magnetization Dynamics in the Single-Molecule Magnet Fe8 under Pulsed Microwave Irradiation. *Phys. Rev. B Condens. Matter Mater. Phys.* **2007**, 75 (6), 1–12.
- (55) Horii, Y.; Katoh, K.; Miyazaki, Y.; Damjanović, M.; Sato, T.; Ungur, L.; Chibotaru, L. F.; Breedlove, B. K.; Nakano, M.; Wernsdorfer, W.; Yamashita, M. Coexistence of Spin–Lattice Relaxation and Phonon-Bottleneck Processes in Gd^{III}–Phthlocyaninato Triple-Decker Complexes under Highly Diluted Conditions. *Chem. A Eur. J.* **2020**, *26* (36), 8076–8082.
- (56) Delaplane, R. G.; Ibers, J. A. Direct Determination of the Effect of Isotopic Substitution on Bond Lengths in Solid Oxalic Acid Dihydrate. *J. Chem. Phys.* **1966**, 45 (9), 3451.
- (57) Rao, C. N. R. Effect of Deuteration on Hydrogen Bonds. J. Chem. Soc. Faraday Trans. 1 Phys. Chem. Condens. Phases 1975, 71, 980–983.
- (58) Eaton, G. R.; Eaton, S. S. Solvent and Temperature Dependence of Spin Echo Dephasing for Chromium(V) and Vanadyl Complexes in Glassy Solution. *J. Magn. Reson.* **1999**, *136* (1), *63*–68.

□ Recommended by ACS

 $\label{eq:conditions} \begin{tabular}{l} Optimized Local Synthetic Conditions Induce Size Reduction and Phase Purification in $\{[Fe(Htrz)_2(trz)](BF_4)\}_n$ Spin Crossover Particles $$$

Tristan Castel, Kevin Bernot, et al.

JANUARY 03, 2023

CRYSTAL GROWTH & DESIGN

READ 🗹

Regulating Magnetic Relaxation of Radical-Ln-Based Chains Involving Multidentate Nitronyl Nitroxides through Varying Spin Arrangement Motif and Local Symmetry around Ln...

Chaoyi Jin, Licun Li, et al.

APRIL 10, 2023

CRYSTAL GROWTH & DESIGN

READ 🗹

Interface versus Bulk Light-Induced Switching in Spin-Crossover Molecular Ultrathin Films Adsorbed on a Metallic Surface

Massine Kelai, Amandine Bellec, et al.

FEBRUARY 14, 2023

THE JOURNAL OF PHYSICAL CHEMISTRY LETTERS

READ 🗹

Variation of the Cooperativity in Diluted Hofmann-Based Spin-Crossover Coordination Solids $\{Fe_{1-x}M_x(pz)[Pd(CN)_4]\}$

Chinmoy Das, Pradip Chakraborty, et al.

APRIL 12, 2023

CRYSTAL GROWTH & DESIGN

READ 🗹

Get More Suggestions >